ARTICLE

Received 00th January 20xx, Accepted 00th January 20xx

DOI: 10.1039/x0xx00000x

Leveraging the Bio-Enabled Muconic Acid Platform Via Phospha-Michael-Addition: Intrinsically Flame-Retardant Nylon-6,6/DOPO copolymers.

Prerana Carter^{a,b}, Peter M Meyer^a, Ting-Han Lee^a, Dhananjay Dileep^a, Nickolas L. Chalgren^a, Sohaima Noreen ^a, Michael J. Forrester ^a, Brent H. Shanks ^{a,b}, Jean-Philippe Tessonnier ^{a,b}, and Eric W Cochran^a

^bCenter for Biorenewable Chemicals (CBiRC), Ames, Iowa, United States

Efforts towards developing biobased chemicals primarily focus on generating molecules chemically analogous to those derived from petroleum. The compositional uniqueness of biomass can also be leveraged to reinvigorate the chemical industry with novel multifunctional molecules. We demonstrate the value and potential of these new compounds in the case of Nylon-6,6, a commodity polyamide that suffers from poor flame resistance. The conventional route to inhibit flammability involves blending the polymer with additives, which can pose health risks due to leaching along with mechanical property trade-offs. Herein, we address these limitations through the synthesis of a novel multifunctional comonomer derived from renewably sourced trans-3-hexenedioic acid (t3HDA). t3HDA was subjected to a one-pot isomerization and functionalization strategy where the alkene migrates to render this molecule active for phospha-Michael-addition (MA) with 9,10-Dihydro-9-Oxa-10-Phosphaphenanthrene-10-Oxide (DOPO), a halogen-free flame-retardant (FR). This DOPO-functional counit was polymerized into Nylon-6,6 copolymers and compared with physical blends of DOPO and Nylon-6,6 using a suite of thermomechanical techniques; analysis revealed comparable crystallinity, flame retardance, and thermomechanical properties for the DOPO-tethered bio-advantaged polyamides. The synthesis strategy presented herein can be extended to a variety of functional groups and novel properties, a platform for creating bespoke bio-advantaged polyamers.

Introduction

Synthetic polymers are ubiquitous to society and have served as the basis for countless advances in the fields of medicine, manufacturing, automotive, and consumer products. Most commodity polymers are derived from fossil-based carbon feedstocks. However, utilization of biomass as a renewable alternative has been gaining prominence due to environmental concerns and growing consumer awareness. These efforts have largely focused on chemically identical replacements for petrochemicals using a bio-feedstock.^{1–3} However, the unique composition of biomass, for instance, the high oxygen content of its building blocks and their distinct stereochemistry, offers opportunities to generate novel chemicals and materials previously unattainable through petroleum.^{4,5}

Biobased platform intermediates that yield both direct replacements and novel molecules were recently identified through reaction network analysis and generation. ^{6–9} The versatility of these bioprivileged compounds allows for their utilization as a platform for the production of bio-derived

commodity chemicals while derisking production of new performance-advantaged molecules. Fermentation-derived muconic acid has received increasing attention due to its bioprivileged nature. Plant platform molecule can be obtained from glucose and lignin derivatives using metabolically-engineered bacteria (*E. coli* and *P. putida* KT2440) or yeast (*S. cerevisiae*). Previous work has demonstrated the diversification of muconic acid to commodity chemicals such as adipic acid, 11,13,16,18-21 hexamethylene diamine, 22 ε-caprolactam, 23,24 and terephthalic acid. Muconic acid-derivatives have additionally been gaining prominence for the production of performance advantaged fiber-reinforced polyesters 28-30 and polyamides. 6,26

The present work is based on the hypothesis that novel monomers derived from muconic acid could be molecularly engineered to become multifunctional, offering more than one target property with a single chemical. This approach could enable the chemical industry to overcome the drawbacks and tradeoffs usually associated with the utilization of additives in polymer manufacturing. For instance, flame retardant (FR) additives are typically blended with polymers to lower their flammability^{31–33} and, therefore, broaden the range of their applications while lowering the risks of personal and property damage in the case of a fire. While vital, these FRs act as plasticizers and lower the mechanical properties of the final product compared to the parent polymer. Moreover, leaching

Electronic Supplementary Information (ESI) available: NMR data, GPC chromatograms, X-ray diffractograms, and additional calorimetry data.

^{a.} Department of Chemical and Biological Engineering, Ames, Iowa, United States

^{b.} Center for Biorenewable Chemicals (CBiRC), Ames, Iowa, United States

ARTICLE Journal Name

reduces their efficacy while presenting environmental and health hazards. 34,35 Here, we explored the potential of trans-3hexenedioic acid (t3HDA), a C6 monounsaturated diacid that is stereoselectively produced by electrochemical hydrogenation of muconic acid.³⁶ We employed the carbon-carbon unsaturation in t3HDA as a tethering point to generate flameinhibiting monomers that imparted improved mechanical properties in Nylon-6,6 (PA66). PA66 is an interesting test case owing to its widespread use as a versatile engineering thermoplastic with excellent thermal stability and hydrogen bonding enhanced mechanical properties.^{37,38} PA66 is found in a wide range of industries including automotives, electronics, films and coatings. Despite its advantages, PA66 suffers from poor flame performance due to its hydrocarbon backbone, giving it an oxygen index value ranging from 21-23%39 and UL 94 rating of V-2.37 The current approach for improving flame performance includes addition of glass and other chemical modifiers in these polyamides to achieve an improved V-0 rating.37,40-42 However, other polymer properties are considerably diminished due to the modifiers and there is potential leaching of chemical additives at high temperatures. The FR candidate that was chosen for this study is 9,10-Dihydro-9-Oxa-10-Phosphaphenanthrene-10-Oxide (DOPO), phosphorus-based FR that has been extensively studied for its superior flame-inhibiting characteristics. 43-45 DOPO exhibits high thermal stability and improved environmental compliance compared to traditionally used brominated FRs. For the synthesis of a DOPO tethered diacid, dimethyl-trans-3hexenedioate (dmt3HD) underwent a base-catalyzed one-pot isomerization and functionalization through Michael-addition (MA). The isomerization of dmt3HD to dimethyl-trans-2hexenedioate (dmt2HD) rendered the molecule active towards MA, consequently allowing DOPO to form a Michael-adduct. The resulting monomer was incorporated into the standard PA66 backbone through copolymerization with adipic acid and hexamethylenediamine. To compare the use of the bio-derived monomer over commercially used FR-blends, a physical mixture between DOPO and PA66 was prepared and characterized. DOPO grafted to the polymer backbone showed a 20% improvement in crystallinity, comparable mechanical properties, and ~8% improvement in flame-inhibition with respect to FR-blended polymers. Overall, this study highlights the potential of using novel bio-derived monomers for performance-advantaged polymers.

Method and Materials

Materials

Dimethyl-trans-3-hexenedioate (dmt3HD), 9,10-Dihydro-9-Oxa-10-Phosphaphenanthrene-10-Oxide (DOPO), and hexamethylene diamine (HMDA) were purchased from TCI America. Dimethyl formamide (DMF), ethyl acetate, methanol, and tetrahydrofuran (THF) were supplied by Fisher Scientific. Triethylamine (TEA), lithium hydroxide (LiOH), deuterium oxide (D2O), trifluoroacetic anhydride (TFAA), and adipic acid (AA) were procured from Sigma-Aldrich. Additionally, nitrogen gas

was purchased from Airgas, deuterated chloroform (CDCl3) and dimethyl sulfoxide-d6 (DMSO-d6) from Cambridge isotopes, and 1,1,1,3,3,3-hexafluoroisopropanol (HFIP) from Oakwood Chemical.

Method

Monomer Synthesis and Purification

A one-pot isomerization, Michael addition, and deesterification was carried out to synthesize the biobased comonomer used in this study. dmt3HD (15 ml) and 1.5 mol equivalent of DOPO (31.07 g) were added to a round bottom flask equipped with a condenser. 20 ml of TEA and 20 ml of DMF served the dual role of solvent and catalyst for isomerization of dmt3HD to dmt2HD and its subsequent Michael addition. The reaction was carried out at 85°C for 4 days (~96 h) under static nitrogen with a stirring rate of 350 rpm. The reaction mixture was analyzed daily by gas chromatography/mass spectrometry (GC/MS) until complete consumption of dmt3/2HD was observed upon which the reaction was stopped. The dimethyl ester groups were subsequently hydrolyzed by adding 4 molar eg. lithium hydroxide in a 5:1 (v/v) water:methanol mixture and reaction for 24 h. Separation of the desired product (DOPO-HDA) was carried out by washing the aqueous layer multiple times with ethyl acetate to remove unreacted DOPO and organic solvents. Finally, DOPO-HDA was precipitated in the aqueous layer through the addition of 2 M HCl until the reaction mixture reached pH 1. DOPO-HDA was extracted using ethyl acetate and the solvent was evaporated to recover the final product. The overall yield after synthesis and purification was 79.9 % measured through 1H-NMR.

Polymerization

Nylon-6,6 salt was prepared by mixing equimolar amounts of AA and HMDA in methanol solutions for 1 h at 40 °C. The precipitated salt was recovered through filtration and was dried overnight in a fume hood. DOPO-functionalized Nylon-6,6 was obtained following a similar procedure. Due to the low solubility of DOPO-HDA in methanol, the salt for this diacid was prepared separately using THF as solvent. Prior to polymerization, the two salts were combined in desired ratios and mixed with 60 wt% DI water to improve mixing. Samples were polymerized in a pressurized microreactor (Parr 4900) equipped with a heating jacket. The temperature was monitored through an external thermocouple. To ensure an inert environment during polymerization, the reactor was purged with nitrogen five times and then pressurized to 150 psig. In the initial stage of the polymerization, the reactor was held at an external set point of 265 °C for 2 h. At the end of this stage, nitrogen and water were vented out. Subsequently, the temperature was increased to 300 °C and held there for 3 h. The mixture was stirred at 400 rpm during the entire polymerization process.

Monomer and Polymer Characterizations

1H-NMR, 13C-NMR, and 31P-NMR spectra were collected with Bruker AVIII600 and NEO 400 spectrometers. Results were analyzed with MestReNova software. About 30-50 mg of monomer and salt samples were dissolved in DMSO-d6 and D2O, respectively. For polyamides, approximately 50 mg of sample were dissolved in a 3:2 (v/v) mixture of CDCI3 and TFAA.

GC/MS was carried out on an Agilent Technologies Model 6890 equipped with a DB-1 column. $1\mu L$ of sample solution was injected with a 3.5 min solvent delay. The temperature was held at 50 °C for 0.2 min, ramped at 12.5 °C/min to 250 °C, and finally ramped at 25 °C/min to 340 °C. Analysis of the MS results was done through AMDIS software (NIST).

Gel Permeation Chromatography

EcoSEC gel permeation chromatography (GPC) system was used to measure polymer molecular weight distributions. The GPC system was equipped with UV and refractive index detectors and consisted of a Tosoh TSKgel SuperH6000 column in series with two Agilent PL HFIP gel columns. Approximately 5 mg polyamide samples were dissolved in 1,1,1,3,3,3-hexafluoroisopropanol (HFIP) and filtered through a 0.45 μm PTFE filter. Sample aggregation and ionic interactions were suppressed by the addition of sodium trifluoroacetate at a concentration of 0.02 mol/L HFIP (1.7 g/kg HFIP). A 10 μL sample volume was injected and analyzed at 45 °C under a 0.3 mL/min flow rate. Mn and Mw of samples were measured using polymethyl methacrylate (PMMA) standards.

Dynamic Scanning Calorimetry (DSC): Thermal characterizations were conducted using a TA DSC Q2500 instrument. Specimens measuring under 5 mg were sealed in hermetic aluminum pans and were cycled thrice under nitrogen over a range of 30 °C to 300 °C with a ramp rate of 10 °C/min. Results were calculated using Trios software from the third cycle to minimize the influence of the polymer's thermal history. Δ Hm was calculated by integrating the melting peak, while Tm and Tc were calculated at the peak of the melting and crystallization events, respectively. The degree of crystallinity χ C_DSC was determined using the following equation:

$$\chi_{C_dsc} = \frac{\Delta H_m}{\Delta H_{f,cyrstal}} * 100\%$$

Where Hf,crystal = 57.8 kJ/mol and refers to the enthalpy of fusion of a single crystal of Nylon-6,6.

Thermogravimetric Analysis (TGA)

TGA measurements were performed in triplicate on a Netzsch STA449 F1 with Proteus software for data analysis. Specimens measuring 5-10 mg were placed in alumina pans. A 5-minute isothermal stage was followed by a 10 °C/min ramp to 800 °C under 20 ml/min nitrogen flow. The decomposition temperature, Td10, was calculated at 10 % mass loss and the residual char was measured at 500 °C. Differential thermogravimetric (DTG) curves were calculated using the first derivative of the TGA data and were plotted as the rate of mass loss versus temperature.

Wide-Angle X-ray Scattering (WAXS)

WAXS patterns were collected for annealed samples using a XENOCS Xeuss 2.0 SWAXS system equipped with Dectris Pilatus3 R 1M detector calibrated using a silver behenate standard. The WAXS measurements were performed under vacuum with the samples fixed directly on the holder. Monochromatized light (λ = 1.54 Å) from Cu K α radiation was used over an acquisition period of 600 s. Results were analyzed with Foxtrot 3.3.4 (SOLEIL Synchrotron, France) for absolute intensity correction of the background signal. The degree of crystallinity (χ c_WAXS) was calculated through the following equation based on the ratio of the area of the crystalline fraction (Ac) to the total area (Aa + Ac) under the WAXS curve.

$$\chi_{c_WAXS} = \frac{Ac}{Ac + Ac} * 100\%$$

Microscale Combustion Calorimetry (MCC)

A micro-combustion calorimeter (MCC) was used to measure the heat of combustion of gases evolved during the controlled pyrolysis of the polyamides. The samples were analyzed under nitrogen using a 1 °C/s heating rate from 200 to 700 °C using method A of ASTM D7309 (pyrolysis under nitrogen). The measurements were performed in triplicate to evaluate their reproducibility. The MCC provided the heat release rate as a function of temperature, where total heat released (THR) was calculated as the area under the curve. Char yield was obtained by measuring the difference in sample mass before and after pyrolysis. Fire growth capacity (FGC) was calculated using ASTM D7309 to provide insights into the potential for the material to ignite and grow in fire intensity once ignited.

Dynamic Mechanical Analysis (DMA)

Polyamide samples in the ISO527-2-1BB geometry were prepared by injection molding under an argon atmosphere using a HAAKE MiniJet Pro. Samples were subsequently annealed under inert conditions at 150 °C for 24 h. Torsional DMA was carried out for annealed samples using a TA Ares G2 instrument. Specimens were heated using a 5 °C/min ramp in the linear viscoelastic regime from 0 °C to 100 °C with an angular frequency of ω = 10 rad s-1. Analysis was performed using Trios software. The storage (E') and loss (E") moduli were measured at 0 °C. The tan (δ) curve was calculated as a ratio between E' and E". Tg values are reported at the peak of the tan (δ).

Tensile Tests

Tensile properties were measured using an Instron Universal Testing Machine (3369 series) with a 10 mm/min extension rate. Triplicates were tested with ISO527-2-1BB geometry and averages were reported.

ARTICLE

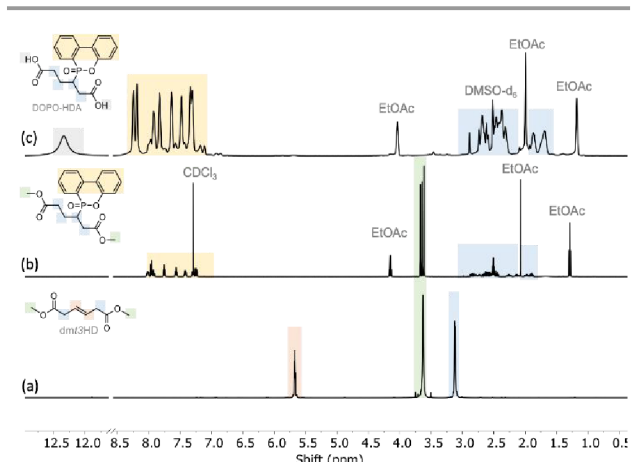
"Scheme 1. Base-catalyzed isomerization of dmt3HD to dmt2HD (Michael acceptor) and its subsequent Michael-addition with DOPO (Michael donor). The diester was hydrolyzed back to the final diacid (DOPO-HDA) prior to polymerization.

Results and Discussion

Synthesis of FR-grafted monomer

A one-pot base-catalyzed isomerization and Michael-addition (MA) was carried out to graft flame-retardant (DOPO) onto dmt3HD (Scheme 1). Equal volumes of TEA and DMF were used to shift the double bond in dmt3HD from the β - γ to α - β position, rendering it active for MA. Subsequently, DOPO underwent a nucleophilic 1,4 phospha-MA onto dmt2HD. This synthesis was performed on the diester (dmt3HD) over the diacid (t3HDA) since the methyl groups prevented ring-closing and formation of lactone by-products under basic conditions. Additionally, t3HDA exhibited limited reactivity towards MA compared to dmt3HD. The selective formation of the desired phospha-MA

Figure 1. 1 H NMR spectra of the (a) starting diester (dmt3HD), (b) DOPO-grafted diester in CDCl₃, (c) and desired product (DOPO-HDA) in DMSO-d₅ quantities of DOPO grafted onto the PA66 backbone (right).



product was confirmed through GC/MS (Figure S1) and 1H-NMR (Figure 1), which showed DOPO-HDA as the sole product. Peaks corresponding to DOPO were observed in the aromatic range of 7–8.5 ppm, whereas the alkene peak of dmt3HD (5.6 ppm) disappeared completely. Recovery of DOPO-HDA was achieved through base-catalyzed hydrolysis (overall yield: 79.9 %) and characterized by 1H-NMR (Figure 1). DOPO-HDA was further utilized for copolymerization and insertion in the Nylon-6,6 backbone.

Table 1. Comparison of theoretical and actual DOPO incorporation into polyamide through ¹H-NMR and molecular weights of polymer series

Samples	Expected mol%	Actual mol% incorporation	Mn ^[b]	Đ
	incorporation (%)	(%) ^[a]	(kDa)	
PA66			65.6	1.78
PAGG	-	-	0.00	1.70
PA66-				
5B	4.8	4.9	78.1	1.79
30	4.0	4.5	70.1	1.19
PA66-5F	4.8	5.0	83.6	1.65
1 700-31	4.0	5.0	00.0	1.00
PA66-				
10B	9.6	8.7	62.3	1.72
PA66-				
10F	9.6	11.0	62.6	1.68

[a] Incorporation of DOPO was calculated through $^1\!H$ NMR analysis of the polymers.

[b] Mn: Number-average molecular weight of polymers were calculated with respect to PMMA standards

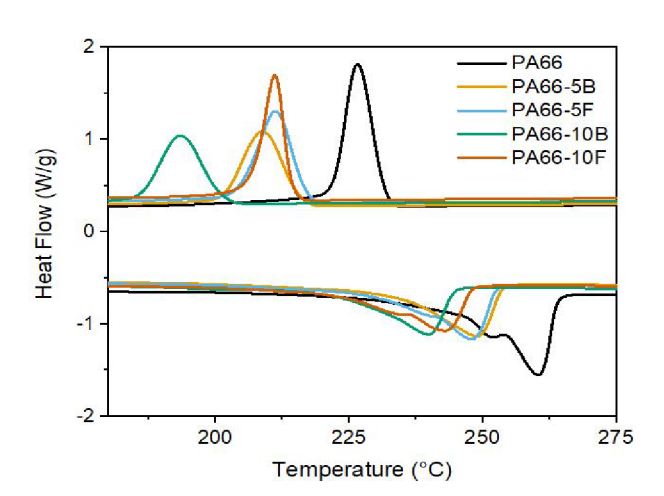
Scheme 2. Polymerization of 5 and 10 wt% DOPO physically blended with PA66 (left) versus equivalent.

Polymerization and characterization of monomer incorporation

Conventional Nylon-6,6 salt was prepared by precipitating HMDA and AA in MeOH. Next, DOPO-nylon blends were prepared by polymerizing the Nylon-6,6 salt in the presence of a desired quantity of DOPO (5 or 10 wt%). This range was selected recognizing the potential adverse impact of

incorporating large quantities of a bulky pendant group on the resulting mechanical properties of the polymer. Post-polymerization, these FR-blended polyamides were referred to as PA66-5B and PA66-10B for the samples containing 5 and 10 wt% DOPO, respectively (Scheme 2). Similarly, a zwitterionic salt was prepared by independently precipitating HMDA and DOPO-HDA in THF (Scheme 2, Figure S2). The novel FR-salt was then mixed with the standard Nylon 6,6 salt in the desired ratios to emulate the DOPO loading in the blends. The polyamides wherein DOPO was tethered to the backbone are referred to as PA66-5F and PA66-10F.

Table 1 compares the theoretical and actual incorporation of DOPO in the polyamide as determined by H-NMR (Figure S3). Actual DOPO incorporation was calculated by integrating the aromatic peaks belonging to DOPO with respect to the HMDA peak at 3.7 ppm. The calculated values confirmed that the concentration of DOPO in the blends and functionalized samples closely followed the expected values (Table 1) and, therefore, the flame-retardant properties of both sample series



 $\begin{tabular}{ll} Figure 2. DSC thermograms for the flame-retardant polyamide series with respect to PA66 showing melting/crystallization event. \end{tabular}$

can be directly compared (vide infra). Additional confirmation for the survival of the grafted DOPO post polymerization was provided by 31P NMR (Figure S4) and the 1H-31P heteronuclear multiple bond correlation (HMBC) spectra presented in Figure S7. PA66-10B exhibited one phosphorus peak showing crosspeaks only in the aromatic region, which substantiated that DOPO remains as a free molecule in the polymer matrix. In contrast, two phosphorus peaks were observed for PA66-10F (Figure S7b). The sharper peak (44 ppm) was associated with the tethered DOPO, established by cross-peaks appearing in both the aromatic and aliphatic regions. The ratio of the two phosphorus peak integrations showed that ~25 % DOPO detached from the polymeric backbone and, therefore, is present as a free molecule such as with the blends. However, as a majority of the DOPO remained attached to the polyamide backbone, differences in properties between blended and functionalized samples are still driven by the tethered groups.

Molecular weight of polymer series

The GPC chromatograms for the polyamide series are shown in Figure S5. The corresponding molecular weights, calculated with respect to PMMA standards, are displayed in Table 1. The extent of DOPO loading (5 wt% versus 10 wt%) had minimal influence on Mn as PA66-5B/10B showed comparable weights intermediate to the PA66 control.

Thermal and crystal properties

The effect of blended and tethered DOPO on thermal properties and crystallinity was investigated through DSC, WAXS, and TGA (Figures 3,4 & S9, Table 2). PA66 exhibited the highest melting temperature (Tm = 260.5 °C) and degree of crystallinity (χC_DSC = 26 %) based on DSC (Figure 2). DOPO incorporation, whether as a blend or a pendant group, inhibited crystal formation and led to a decrease in Tm and χC_DSC. While PA66-5B/5F exhibited similar DHm and Tm, a prominent difference was observed with the higher DOPO loaded samples. PA66-10B showed the lowest Tm (239.7 °C) and χC_DSC (15 %). In contrast, the tethering of DOPO to the PA66 backbone in the 10F sample showed superior crystallinity of over 18 %. To evaluate the crystalline structure, room temperature WAXS was performed on polymer samples annealed for 24 h (Figure S9). The semi-crystalline nature of these polyamides was established by the sharp peaks representing crystalline segments and the characteristic broad halo corresponding to the amorphous regions. The percent crystallinity (χC_WAXS) is ARTICLE Journal Name

reported as the ratio of the areas under the peaks normalized over the total area. PA66 exhibited two characteristic peaks at approximately 20° and 24° , corresponding to the (100) and (010)/(110) doublet of the α -phase. PA66 possesses a triclinic structure, in which the (100) peak represents intrasheet scattering caused by adjacent polymer chains in a sheet and the (010)/(110) peak corresponds to the intersheet scattering between polymer sheets. Following the results from DSC, it was expected that both modes of DOPO incorporation would retard crystallization. While that effect was observed, the difference in % crystallinity between blends and functionalized samples was

amplified post polymer annealing. In the case of the blended specimens at 5 and 10 wt% loadings (PA66-5/10B), the polymers showed a decrease in crystallinity to 35.0 % and 31.8 % respectively compared to 42.2% in neat PA66. In contrast, the functionalized samples PA66-5/10F were within 10% of the PA66 value at 38.8%/38.2%. In both cases, expulsion of free DOPO and functionalized DOPO segments to the amorphous phase was anticipated. However, annealing for sufficient time above the glass-transition temperature allowed PA66-5/10F to have higher thermodynamic preference for crystallization compared to the blends (Figure S8).

Table 2. Thermal properties of the polyamides with different loadings of DOPO as blends or tethered into the backbone.

	DSC Analysis			WAXS	TGA Analysis				
	$T_{\scriptscriptstyle m m}^{\scriptscriptstyle [a]}$	ΔHm	$\chi_{\text{c_DSC}}$	T_c	X _{c_WAXS} ^[b]	Char _{soo*c} [c]	$T_{\scriptscriptstyle m d10}$	DTG peak(s) ^[d]	
Sample	(°C)	(J/g)	(%)	(°C)	(%)	(%)	(°C)	Peak 1(°C)	Peak 2(°C)
PA66	260.5	66.4	26.0	226.7	42.2	3.04 ± 1.4	487.2 ± 0.3	448.4 ± 3.6	-
PA66-5B	248.8	50.8	19.9	208.8	35.0	4.05 ± 0.6	330.7 ± 4.0	391.2 ± 0.2	466.2 ±1.6
PA66-5F	247.9	49.5	19.4	211.2	38.8	4.04 ± 0.3	325.0 ± 3.5	393.5 ± 1.9	462.3 ± 3.1
PA66-10B	239.7	38.2	15.0	193.3	31.8	3.96 ± 0.8	327.5 ± 5.2	377.2 ± 0.2	458.3 ± 7.8
PA66-10F	242.9	46.8	18.3	211.0	38.2	4.57 ± 0.2	302.7 ± 2.3	384.4 ± 1.3	463.5 ± 0.3

- [a] T_m : melting temperature; ΔH_m : enthalpy of melting; T_c : crystallization temperature; $\chi_{c.DSC}$: percent crystallinity (DSC).
- [b] $\chi_{c,waxs}$: percent crystallinity from WAXS (annealed).
- [c] Char_{500 °C}: residual mass at 500 °C; T_{d10} , decomposition temperature at 10% mass loss under N_2 from TGA.
- [d] DTG peaks: calculated from the derivative of TGA curves.

Thermogravimetric analysis (TGA) was performed on PA66 and FR polyamides to investigate the influence of DOPO on thermal decomposition and flame inhibition (Figure 3a).36 The DTG curve (1st derivate of the TGA curve) shows thermal decomposition events more prominently (Figure 3b). PA66 showed one decomposition peak consistent with the literature, whereas polymers containing DOPO exhibited two decomposition events. The first stage corresponds to the evolution of DOPO out of the polymer matrix, which is corroborated by the boiling point of DOPO reported at ~380 °C.

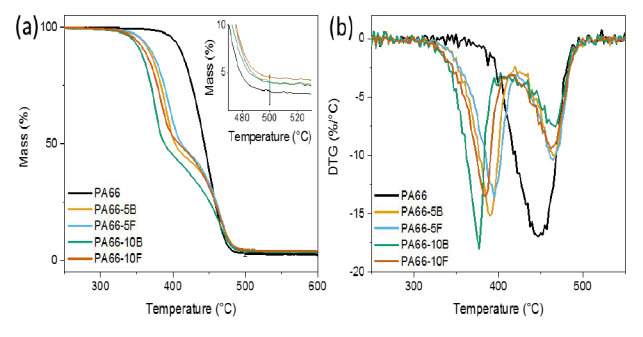


Figure 3. (a) TGA thermograms and (b) DTG curves showing a single step decomposition for PA66 and a two-stage decomposition of FR polyamides. Samples were run in triplicates under nitrogen with a $10\,^{\circ}\text{C/min}$ ramp rate.

Tethering DOPO to the polymer backbone allowed it to evolve marginally later compared to the DOPO blended samples. This is demonstrated in Table 2 where PA66-10B showed its 1st decomposition peak 8 °C lower than its tethered counterpart (PA66-10F). From Figure 3a and Table 2, char yield for all samples containing DOPO increased compared to PA66. Phosphorus is known to promote char formation through phosphoric acid derivatives, which in turn may act as crosslinkers to decomposed polymeric byproducts.42 The char layer subsequently acts as a mass and heat transfer barrier to slow flame spread.42 Char yield was seen to be the highest for the 10F sample, which could be the result of tethering DOPO to the polyamide backbone and allowing it to interact with the solid phase. Therefore, tethering FR to polymeric backbone reduced volatilization of the FR and enabled it to increase interaction with the condensed phase.

Flame-inhibition analysis

MCC was used to measure the heat release rate (HRR) versus temperature to gauge flame performance for the polyamide series (Figure 4). Compared to the PA66 control sample, all DOPO-containing materials showed improvements in terms of heat release and char yield (Table S1, Figure S6). In contrast to PA66, the FR-samples showed two peaks of heat release, which indicates that DOPO chemistry is changing the thermal

Table 3. Viscoelastic properties of polyamides measured through torsional DMA.

Sample	E' @ 0 °C (GPa)	E" @ 0 ∘C (MPa)	$T_{g_{LDM4}}$ (°C)
PA66	1.86	9.5	71.6
PA66-5B	1.94	6.2	79.9
PA66-5F	1.94	9.9	83.1
PA66-10B	2.40	3.9	80.8
PA66-10F	2.32	6.9	90.3

decomposition characteristics of the polyamides. Fire growth capacity (FGC) is a parameter calculated through ASTM D7309, which is dependent on chemical structure and gives insights into ignition and flame-growth once ignited.43 The FGC of PA66 decreased from 500 J/g-K to 327.5 J/g-K for PA66-10B and 302.6 J/g-K for PA66-10F. Additionally, a large reduction in peak HRR was observed for the PA66-10B and PA66-10F showing that higher loadings of DOPO enhance flame inhibition (Table S1). Overall, it can be seen that DOPO enhanced flame-retardance compared to neat PA66, however its mode of incorporation affected polymer performance minimally. A more drastic difference might be expected between blends and tethered FRs if lower boiling point modifying chemicals are used.

Rheology and Mechanical Properties

Torsional dynamic mechanical analysis (DMA) was conducted to understand the viscoelastic response of the annealed polyamides to a known deformation as a function of temperature (Figure 5). Values for the storage modulus (E'), loss modulus (E"), and tan δ are summarized in Table 3. E' and E" were reported at the glassy plateau of 0 °C. Tan δ is calculated through the ratio between E' and E'', where δ is the phase angle between the stress and the strain. In this study, the glasstransition temperature of the polymers (Tg) was located using the maxima of tan δ . Tg is a key polymer property and is characterized as the temperature at which long-range motion in the amorphous domains ceases as a polymer melt is cooled. Over this transition, dramatic changes in properties are observed as the polymer shifts from a rubbery to glassy state.PA66 showed the lowest E', followed by PA66-5B/F. A slight reduction in E' was also observed for the 10F sample relative to 10B, potentially due to their reduced Mn. However, a significant increase in Tg (~10 °C) was observed between PA66-10B and 10F. In the blends, free DOPO molecules act as plasticizers in the amorphous domains of the polymer. This

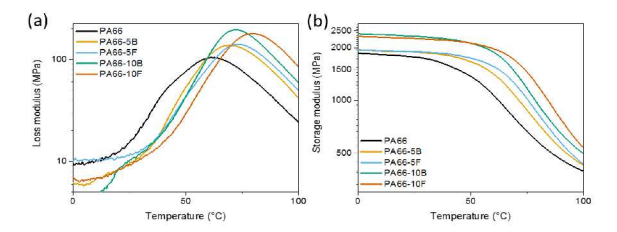


Figure 5. (a) Loss and (b) storage modulus of polyamide samples with different modes of DOPO incorporation.

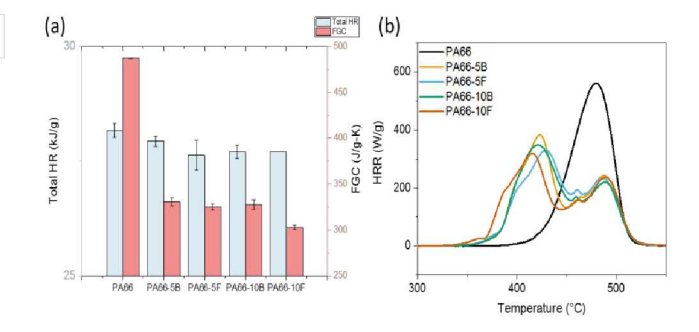


Figure 4. Comparison of combustion characteristic of polymers in this study. (a) Total HR was shown to decrease with DOPO containing samples. PA66-F samples showed a lower FGC compared to PA66-B specimens. (b) HRR versus temperature for triplicates

enables chain mobility at lower temperatures, which is revealed by the suppressed Tg exhibited by the blends. In contrast, when DOPO is tethered to the polyamide backbone, chain mobility and diffusivity are reduced due to the anchored pendant group. This effect is observed through the consistently increased Tg in both functionalized samples (5F/10F) compared to their corresponding blends.

Mechanical properties of the samples were assessed using tensile tests that were run in triplicate (Table 4). Mechanical properties of polymers are related to the crystallinity and molecular weights of the samples. At 5% loading, the functionalized sample (5F) showed a significantly higher UTS and Young's modulus compared to both neat PA66 and PA66-5B. This could be explained in part due to the suppressed crystallization in the 5B sample compared to the 5F sample. This trend did not extend to the 10 wt% DOPO samples, however. The 10F samples were significantly more brittle than others, which is reflected in the lower tensile toughness values and the large variance in the UTS value. We note that these samples were tested bone dry and without added plasticizer. Atmospheric moisture is well known to plasticize PA66, significantly reducing its brittleness.⁴⁶ In the future, retesting with larger tensile specimen conditioned in a humidified environment would provide a complementary picture of how these materials could be expected to perform under everyday use conditions.

Table 4. Mechanical properties of polymer specimens (triplicates) as determined through tensile testing.

Samples	UTS (MPa)	Toughness (MPa)	Young's Modulus (GPa)	Elongation at break (%)
PA66	84.2 ± 10.6	3.69 ± 1.03	1.18 ± 0.00	8.03 ± 1.20
PA66-5B	89.0 ± 13.0	3.50 ± 1.10	1.47 ± 0.00	7.25 ± 1.20
PA66-5F	129± 6.40	9.97 ± 3.90	1.47 ± 0.01	12.7 ± 2.80
PA66-10B	90.4 ± 4.50	3.39±0.420	1.56 ± 0.01	7.02 ± 0.50
PA66-10F	68.7 ± 24.9	2.15 ± 1.17	1.46 ± 0.22	5.50 ± 1.3

ARTICLE Journal Name

Conclusions

Utilization of bio-based molecules can be leveraged to give access to novel multifunctional monomers that are key towards producing performance-advantaged polymers. Demonstrated in this study is the potential of a multifunctional monomer produced using fermentation-derived t3HDA for flameretardant applications. Currently, flame-retardance in polymers is primarily achieved through physical blending of flameretardant molecules. However, this approach can lead to leaching of the FRs that ultimately diminish flame-inhibiting performance and also detrimentally affect mechanical properties in the polymer caused by the disruption in crystal formation. To address these drawbacks, a novel diacid was prepared by tethering FR molecule DOPO onto the unsaturation offered by t3HDA and copolymerized into a Nylon-6,6 backbone. For equivalent comparison, PA66 was physically blended with DOPO and the impact of the two modes of DOPO incorporation on polymer properties was investigated. Tethering the FR group achieved improved flame retardance at higher loadings compared to FR blends. However, significant improvements in crystallinity were offered by DOPOfunctionalized polyamides over the blends. χc was minimally affected compared to neat PA66 and its effect was observed through improved mechanical properties when molecular weights were comparable. As the DOPO segments and free molecules were relegated to the amorphous regions, properties observed via DMA seemed to be affected compared to neat PA66. Tg and E' were increased due to the rigidity offered by the aromatic rings in DOPO. This study leverages bio advantaged and bio privileged concepts and uses t3HDA as a vehicle for inserting flame-retardance while minimally compromising on other key polymer properties. Extension of this chemistry would create new opportunities to investigate halogen-free nitrogen and phosphorus-based FRs that were previously not considered due their volatility as free molecules.⁴⁷ Furthermore, the synthesis framework can be used to accelerate development of biopolymers by allowing selective alteration of polymer properties.

Author Contributions

Prerana Carter, PhD (Data curation: Equal; Formal analysis: Equal; Investigation: Lead; Methodology: Equal; Visualization: Equal; Writing – original draft: Lead); **Peter M Meye**r (Data curation: Equal; Formal analysis: Equal; Investigation: Equal; Visualization: Equal; Writing - review & editing: Lead); Michael J Forrester, PhD (Data curation: Supporting; Formal analysis: Equal; Investigation: Supporting; Methodology: Supporting; Supervision: Supporting; Writing – review & editing: Equal); **Dhananjay Dileep** (Data curation: Supporting; Formal analysis: Supporting; Methodology: Supporting) ; Ting-Han Lee, PhD (Data curation: Supporting; Investigation: Supporting; Methodology: Supporting); Sohaima Noreen (Data curation: Supporting); Nickolas L Chalgren (Data curation: Supporting); Brent Shanks, PhD (Conceptualization: Equal; Project administration: Lead; Resources: Lead; Supervision: Equal; Writing review & editing: Supporting); Jean-Phillippe Tessonnier, PhD (Conceptualization: Equal; Supervision: Equal; Writing - review &

editing: Equal); **Eric Cochran, PhD** (Conceptualization: Equal; Data curation: Supporting; Formal analysis: Supporting; Funding acquisition: Supporting; Investigation: Supporting; Methodology: Supporting; Writing – original draft: Supporting; Writing – review & editing: Equal).

Conflicts of interest

There are no conflicts to declare

Acknowledgements

This material is based upon work supported by the U.S. Department of Energy's Office of Energy Efficiency and Renewable Energy (EERE) under the Bioenergy Technologies Office Award Number DE-EE0008492. We thank Dr. Sarah Cady (ISU Chemical Instrumentation Facility) for training and assistance pertaining to the NMR results included in this publication.

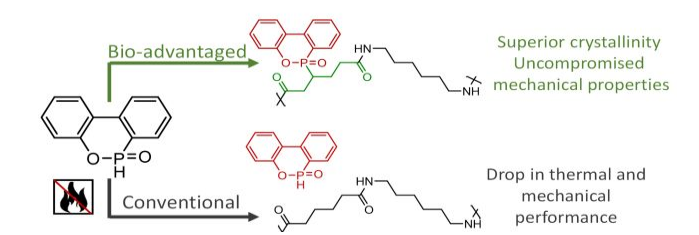
Notes and references

- 1 E. S. Lipinsky, Science, 1981, 212, 1465–1471.
- 2 S. Choi, C. W. Song, J. H. Shin and S. Y. Lee, *Metabolic Engineering*, 2015, **28**, 223–239.
- 3 S. Takkellapati, T. Li and M. A. Gonzalez, *Clean Techn Environ Policy*, 2018, **20**, 1615–1630.
- 4 N. Fitzgerald and A. Bailey, Moving Beyond Drop-In Replacements: Performance-Advantaged Biobased Chemicals, 2018.
- 5 R. M. Cywar, N. A. Rorrer, C. B. Hoyt, G. T. Beckham and E. Y.-X. Chen, *Nat Rev Mater*, 2022, **7**, 83–103.
- 6 J. Huo and B. H. Shanks, *Annu. Rev. Chem. Biomol. Eng.*, 2020, **11**, 63–85.
- 7 X. Zhou, Z. J. Brentzel, G. A. Kraus, P. L. Keeling, J. A. Dumesic, B. H. Shanks and L. J. Broadbelt, *ACS Sustainable Chem. Eng.*, 2019. **7**. 2414–2428.
- 8 B. H. Shanks and P. L. Keeling, *Green Chem.*, 2017, **19**, 3177–3185.
- 9 B. H. Shanks and L. J. Broadbelt, *ChemSusChem*, 2019, cssc.201900323.
- 10 I. Khalil, G. Quintens, T. Junkers and M. Dusselier, *Green Chem.*, 2020, **22**, 1517–1541.
- 11 United States, US5487987A, 1996.
- 12 K. A. Curran, J. M. Leavitt, A. S. Karim and H. S. Alper, *Metabolic Engineering*, 2013, **15**, 55–66.
- 13 D. R. Vardon, M. A. Franden, C. W. Johnson, E. M. Karp, M. T. Guarnieri, J. G. Linger, M. J. Salm, T. J. Strathmann and G. T. Beckham, *Energy Environ. Sci.*, 2015, **8**, 617–628.
- 14 M. Suástegui and Z. Shao, *J Ind Microbiol Biotechnol*, 2016, **43**, 1611–1624.
- 15 M. Suastegui, J. E. Matthiesen, J. M. Carraher, N. Hernandez, N. Rodriguez Quiroz, A. Okerlund, E. W. Cochran, Z. Shao and J.-P. Tessonnier, *Angew. Chem. Int. Ed.*, 2016, **55**, 2368–2373.
- 16 US8592189B2,
- 17 H. Almqvist, H. Veras, K. Li, J. Garcia Hidalgo, C. Hulteberg, M. Gorwa-Grauslund, N. Skorupa Parachin and M. Carlquist, *ACS Sustainable Chem. Eng.*, 2021, acssuschemeng.1c00933.
- 18 D. R. Vardon, N. A. Rorrer, D. Salvachúa, A. E. Settle, C. W. Johnson, M. J. Menart, N. S. Cleveland, P. N. Ciesielski, K. X. Steirer, J. R. Dorgan and G. T. Beckham, *Green Chem.*, 2016, **18**, 3397–3413.
- 19 S. Capelli, D. Motta, C. Evangelisti, N. Dimitratos, L. Prati, C. Pirola and A. Villa, *ChemCatChem*, 2019, **11**, 3075–3084.

- 20 J. E. Matthiesen, J. M. Carraher, M. Vasiliu, D. A. Dixon and J.-P. Tessonnier, *ACS Sustainable Chem. Eng.*, 2016, **4**, 3575–3585.
- 21 W. Niu, K. M. Draths and J. W. Frost, *Biotechnol. Prog.*, 2002, **18**, 201–211.
- 22 World Intellectual Property Organization, WO2015086819A1, 2015.
- 23 20130085255, 2013.
- 24 R. Beerthuis, G. Rothenberg and N. R. Shiju, *Green Chem.*, 2015, **17**, 1341–1361.
- 25 D. I. Collias, A. M. Harris, V. Nagpal, I. W. Cottrell and M. W. Schultheis, *Industrial Biotechnology*, 2014, **10**, 91–105.
- 26 J. M. Carraher, T. Pfennig, R. G. Rao, B. H. Shanks and J.-P. Tessonnier, *Green Chem.*, 2017, **19**, 3042–3050.
- 27 R. Lu, F. Lu, J. Chen, W. Yu, Q. Huang, J. Zhang and J. Xu, *Angew. Chem. Int. Ed.*, 2016, **55**, 249–253.
- 28 N. A. Rorrer, S. Nicholson, A. Carpenter, M. J. Biddy, N. J. Grundl and G. T. Beckham, *Joule*, 2019, **3**, 1006–1027.
- 29 N. A. Rorrer, J. R. Dorgan, D. R. Vardon, C. R. Martinez, Y. Yang and G. T. Beckham, *ACS Sustainable Chem. Eng.*, 2016, **4**, 6867–6876.
- 30 N. A. Rorrer, D. R. Vardon, J. R. Dorgan, E. J. Gjersing and G. T. Beckham, *Green Chem.*, 2017, **19**, 2812–2825.
- 31 B. A. Howell, K. L. Oberdorfer and E. A. Ostrander, *International Journal of Polymer Science*, 2018, **2018**, e7237236.
- 32 B. A. Howell, K. E. Carter and H. Dangalle, in *Renewable and Sustainable Polymers*, American Chemical Society, 2011, vol. 1063, pp. 133–152.
- 33 B. A. Howell and W. Sun, *Polymer Degradation and Stability*, 2018, **157**, 199–211.
- 34 A. Blum and B. N. Ames, Science, 1977, 195, 17-23.
- 35 A. B. Morgan, *Polymer Reviews*, 2019, **59**, 25–54.
- 36 M. N. Dell'Anna, M. Laureano, H. Bateni, J. E. Matthiesen, L. Zaza, M. P. Zembrzuski, T. J. Paskach and J.-P. Tessonnier, *Green Chem.*, 2021, **23**, 6456–6468.
- 37 M. I. Kohan, Ed., *Nylon plastics handbook*, Hanser Publishers; Distributed in the USA and in Canada by Hanser/Gardner Publications, Munich; New York: Cincinnati, 1995.
- 38 M. Winnacker and B. Rieger, *Macromol. Rapid Commun.*, 2016, **37**, 1391–1413.
- 39 D. W. van Krevelen, *Polymer*, 1975, **16**, 615–620.
- 40 E. Braun and B. C. Levin, Fire and Materials, 1987, 11, 71-88.
- 41 U. Braun, B. Schartel, M. A. Fichera and C. Jäger, *Polymer Degradation and Stability*, 2007, **92**, 1528–1545.
- 42 M. S. Subbulakshmi, N. Kasturiya, Hansraj, P. Bajaj and A. K. Agarwal, *Journal of Macromolecular Science, Part C: Polymer Reviews*, 2000, **40**, 85–104.
- 43 K. A. Salmeia and S. Gaan, *Polymer Degradation and Stability*, 2015, **113**, 119–134.
- 44 X. Wang, Y. Hu, L. Song, W. Xing, H. Lu, P. Lv and G. Jie, *Polymer*, 2010, **51**, 2435–2445.
- 45 J. Sag, P. Kukla, D. Goedderz, H. Roch, S. Kabasci, M. Döring and F. Schönberger, *Polymers*, 2020, **12**, 778.
- 46 J. Sag, D. Goedderz, P. Kukla, L. Greiner, F. Schönberger and M. Döring, *Molecules*, 2019, **24**, 3746.
- 47 Y. Cao, X.-L. Wang, W.-Q. Zhang, X.-W. Yin, Y.-Q. Shi and Y.-Z. Wang, *Ind. Eng. Chem. Res.*, 2017, **56**, 5913–5924.

In response to urgent global calls for sustainable industrial practices, this study introduces a transformative approach to synthesizing flame-retardant polyamides that significantly advances environmental sustainability. Addressing the critical issue of flammability in Nylon-66, a widely used polymer, our work circumvents the need for hazardous, leaching-prone additives by incorporating a novel, renewably sourced comonomer derived from muconic acid. This bio-based innovation mitigates health risks while preserving the mechanical integrity of the material, showcasing an exemplary case of enhancing safety without compromising performance. Aligned with the United Nations Sustainable Development Goals, particularly Goal 9 (Industry, Innovation, and Infrastructure) and Goal 12 (Responsible Consumption and Production), our research demonstrates how leveraging biobased solutions can lead to safer, more sustainable materials. The synthesis strategy presented paves the way for the development of a new class of biobased polymers with tailored properties, marking a significant step toward reducing our reliance on fossil fuels and enhancing the environmental resilience of the chemical industry.

Entry for the Table of Contents



We report on a new bio-advantaged molecule capable of tethering flame-retardant additives such as 9,10-dihydro-9-oxa-10-phosphaphenanthrene-10-oxide (DOPO) to the backbone of a polyamide through trans-3-hexenedioic acid (t3HDA) a bioadvantaged derivative of muconic acid.

Supporting Information

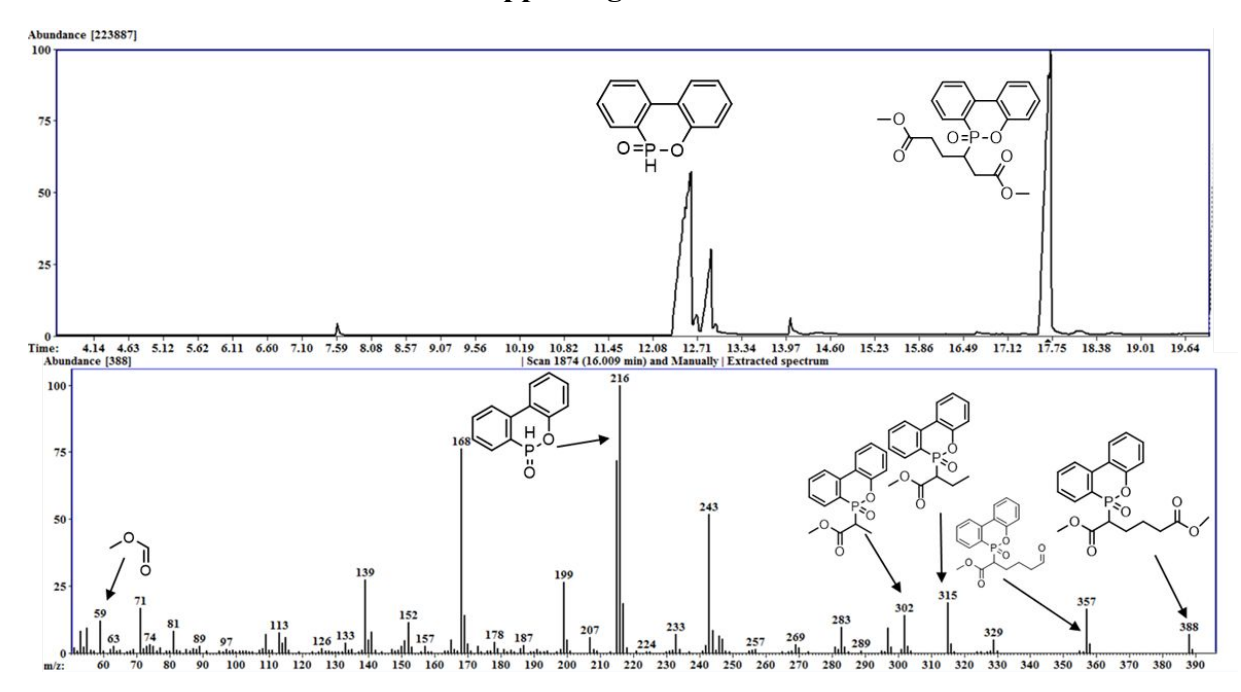


Figure S1. GC-MS for the one-pot isomerization and Michael-addition product after 96 hours of reaction time.

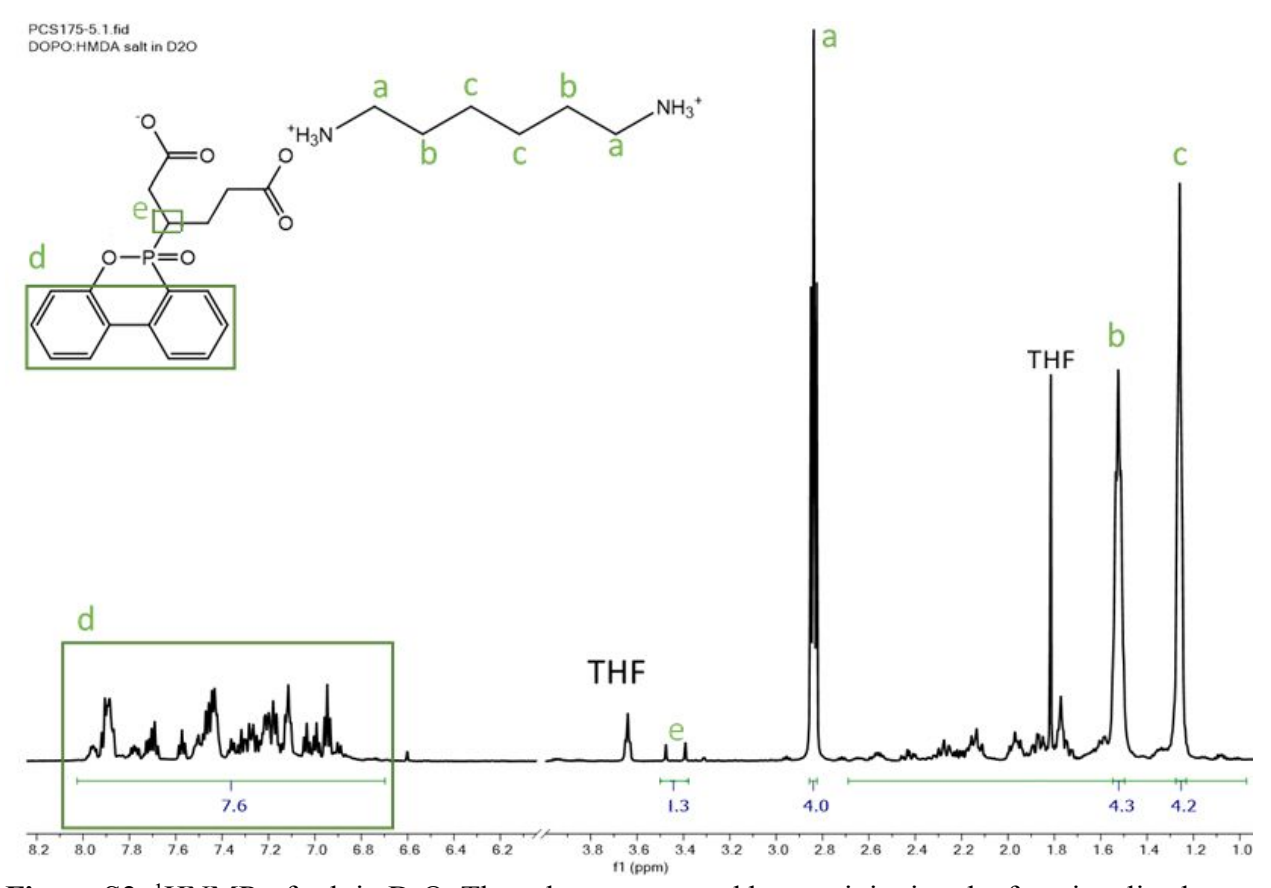


Figure S2. 1 HNMR of salt in $D_{2}O$. The salt was prepared by precipitating the functionalized diacid with HMDA in THF.

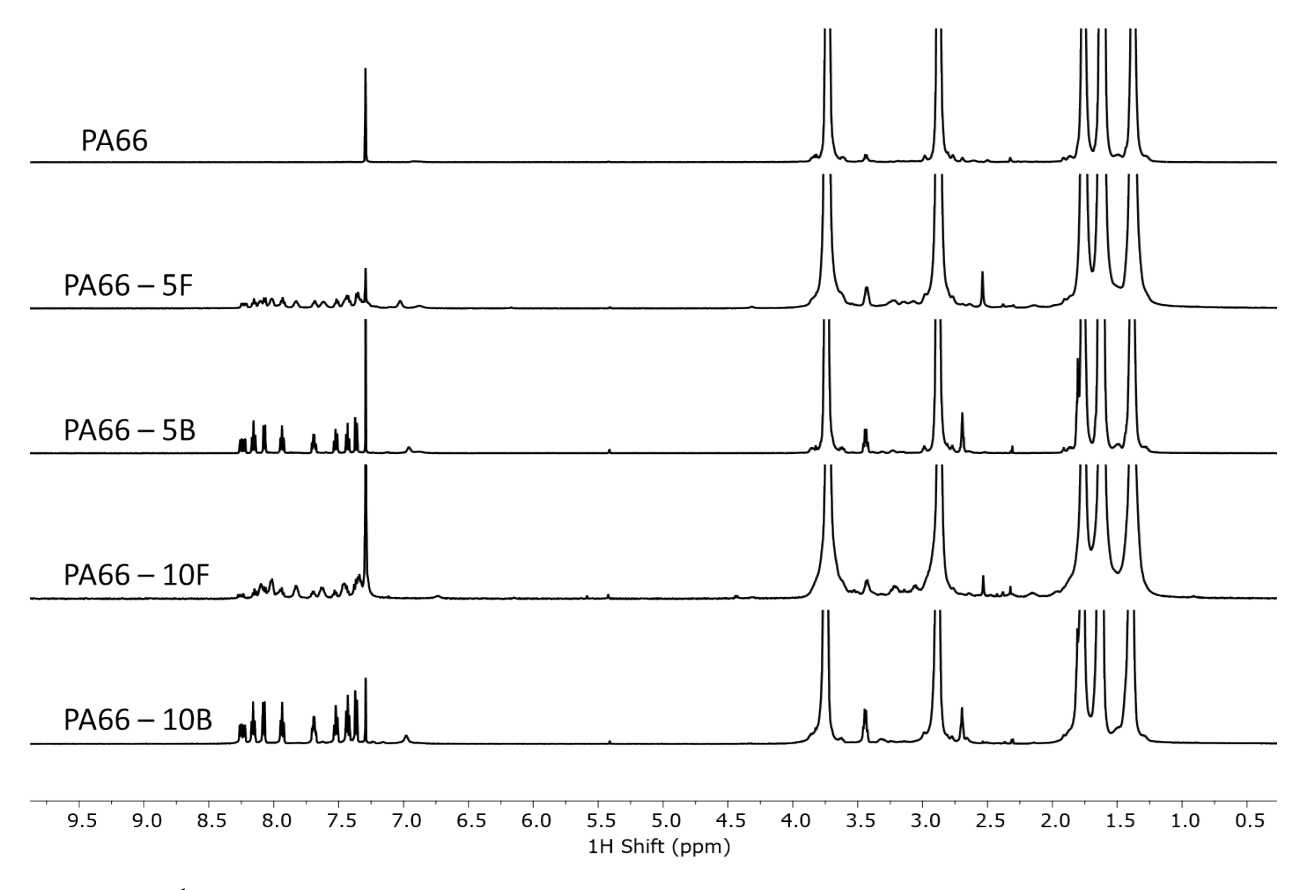


Figure S3. ¹HNMR of polymers shown in this study. Percent incorporation of DOPO was calculated through the integration of the aromatic region with respect to the HMDA peak at 3.7 ppm.



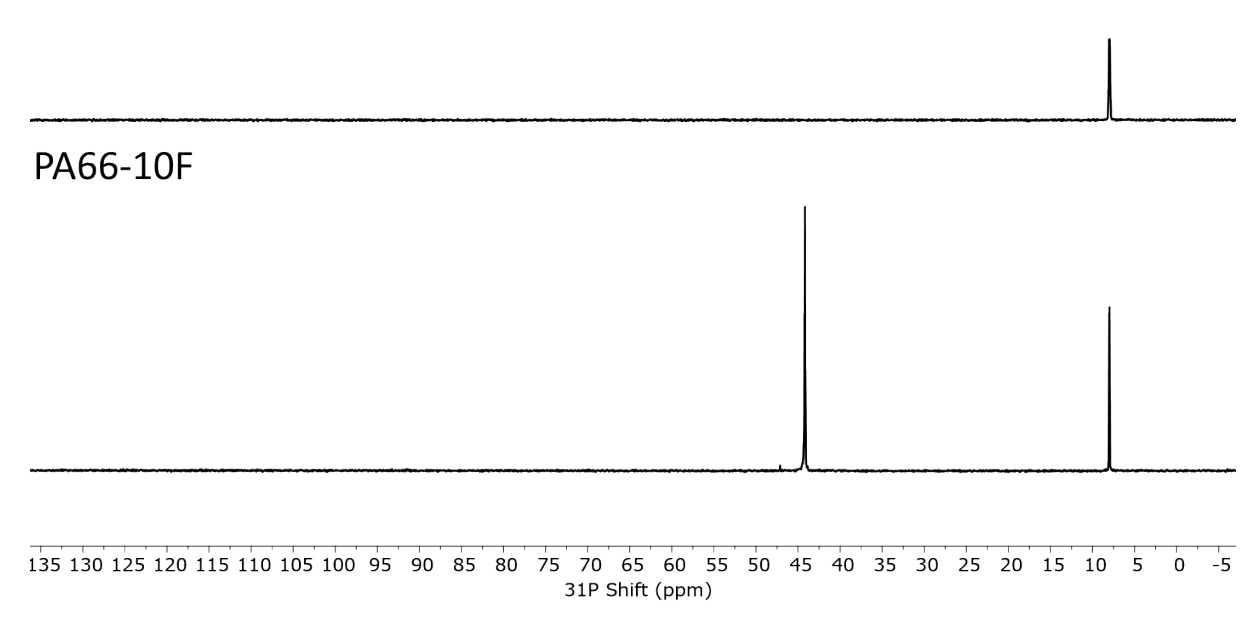


Figure S4. ³¹P-NMR of polymers with 10 wt% DOPO incorporation.

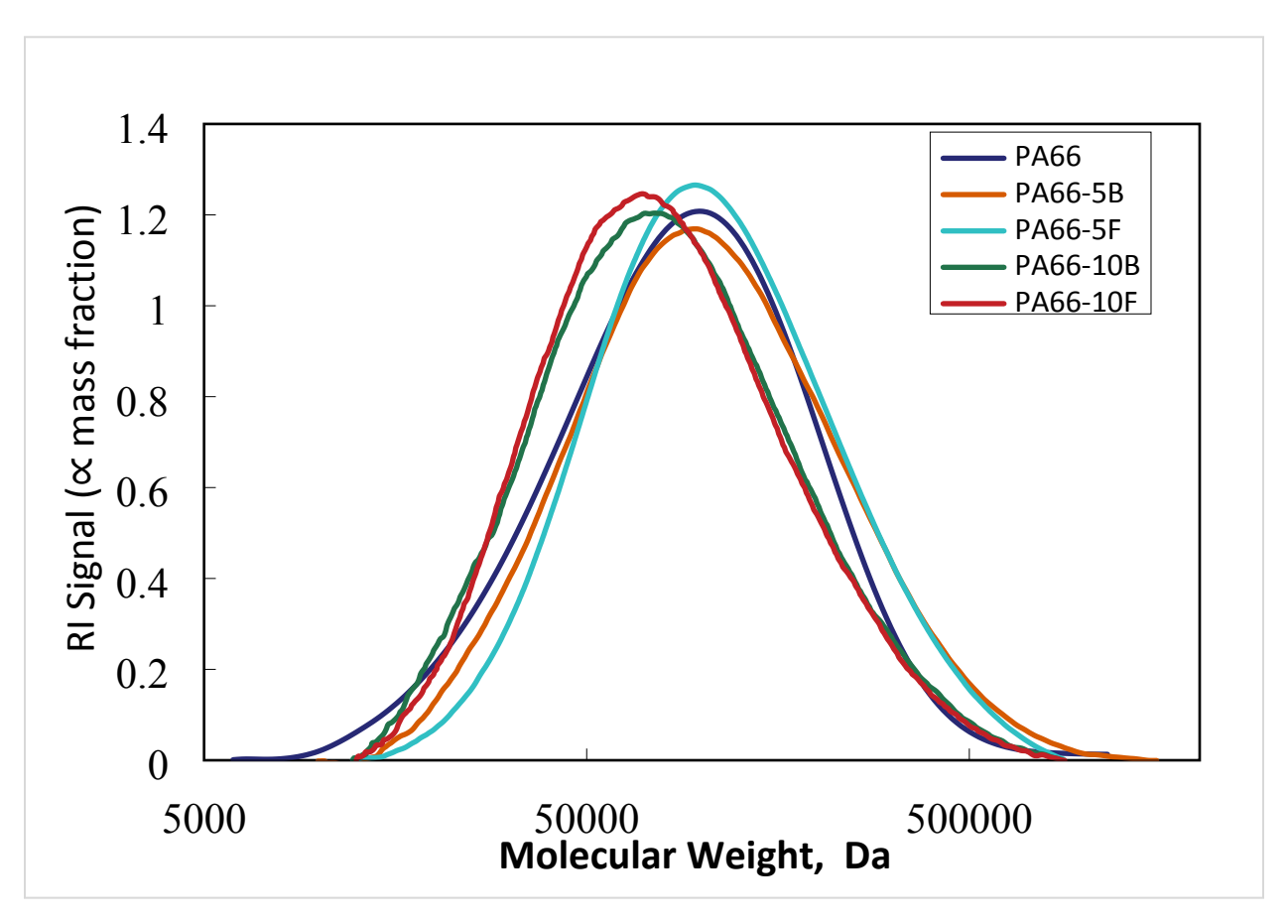


Figure S5: GPC chromatograms for the polyamide series, normalized to unit area.

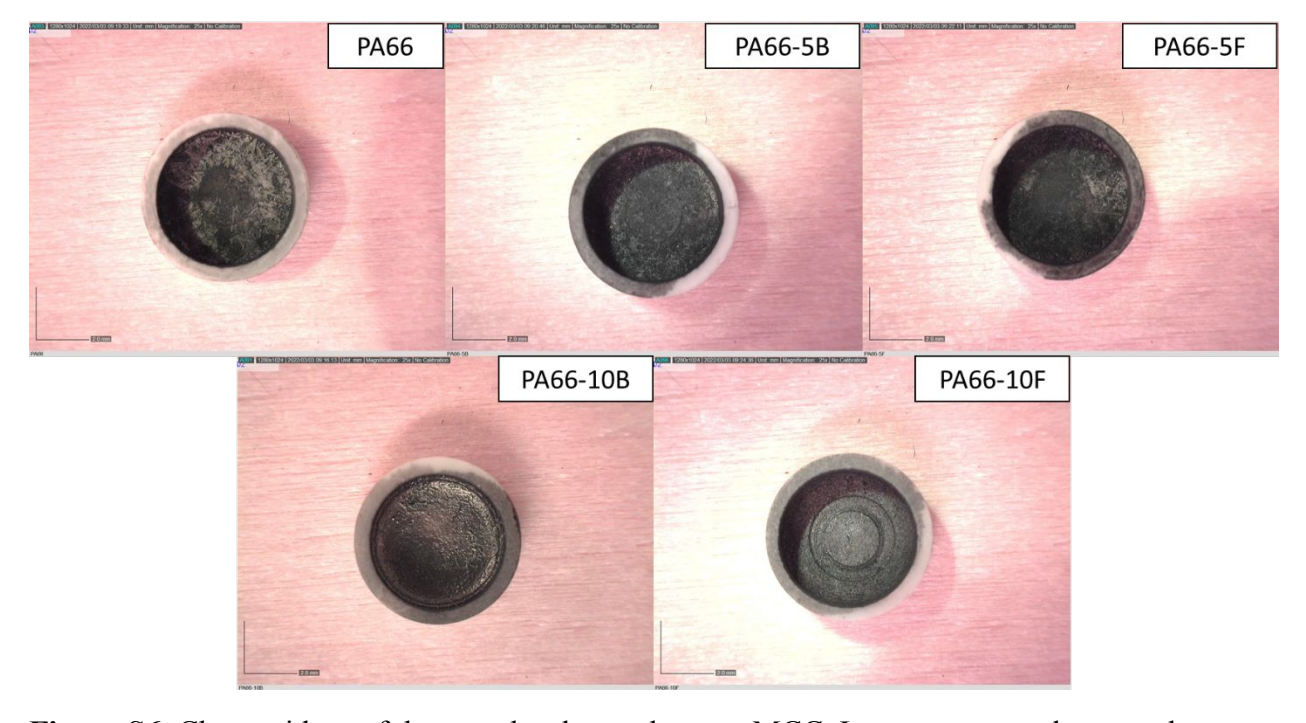


Figure S6. Char residues of the samples that underwent MCC. Images suggest that samples flowed before charring and flowed up to the edges of crucibles prior to being fully pyrolyzed.

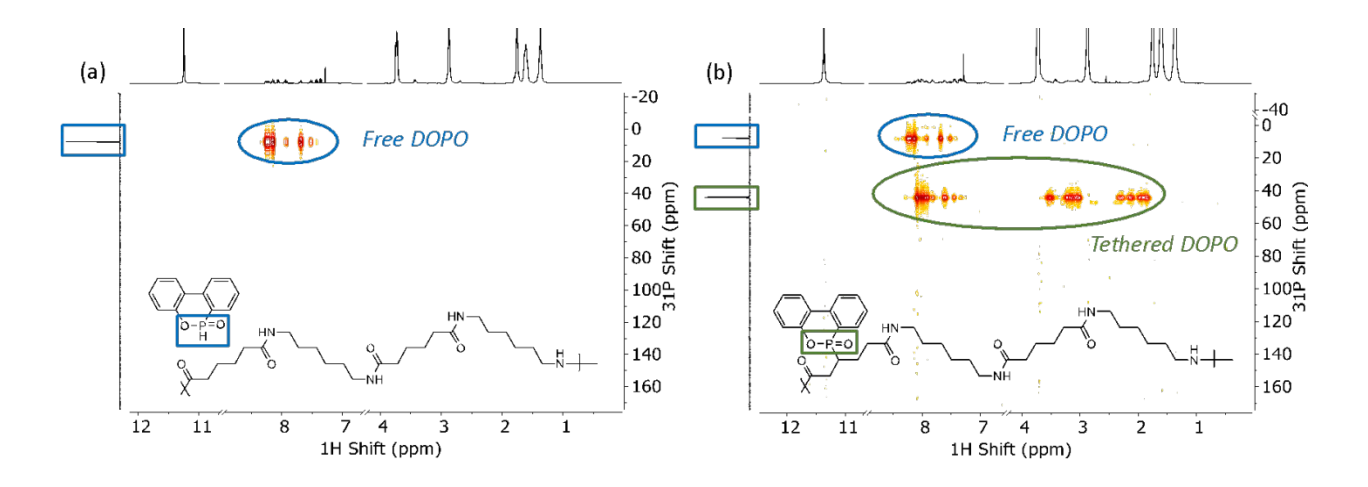


Figure S7. HMBC spectra of ³¹P versus ¹H for (a) PA66-10B and (b) PA66-10F in CDCl₃. The appearance of cross peaks highlighted in green in (b) shows the majority (75%) of DOPO remains grafted onto the polymer backbone during polymerization.

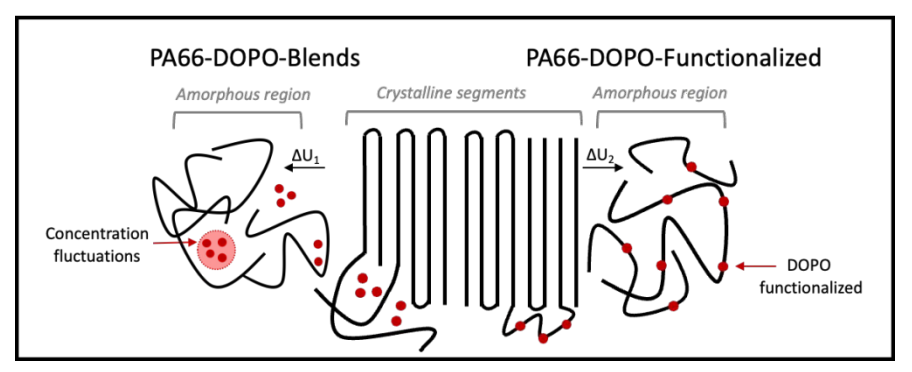


Figure S8. Crystal formation in the presence of free and tethered DOPO. Functionalized DOPO attached to the polymer backbone shows higher crystallinity than its blended counterpart.

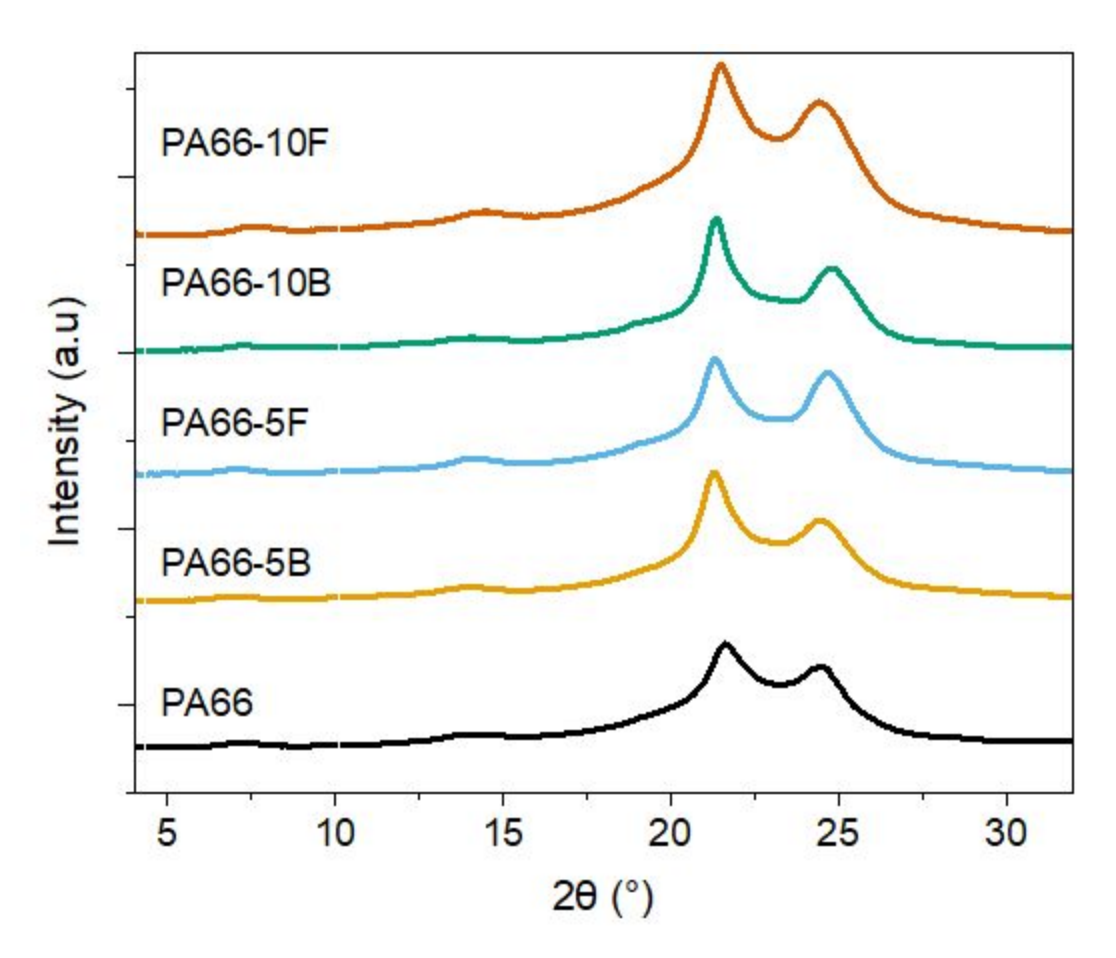


Figure S9: WAXS for the flame-retardant polyamide series with respect to PA66 showing room temperature wide-angle X-ray scattering.

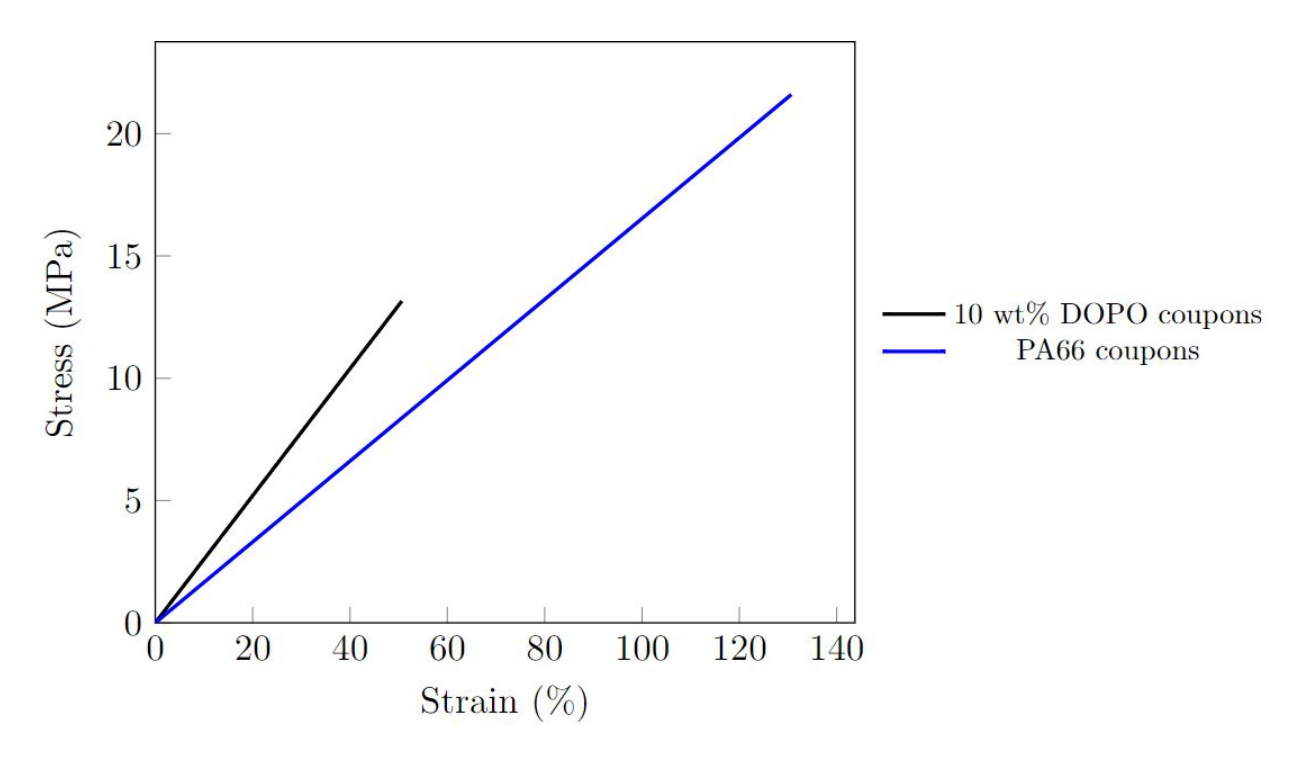


Figure S10: Mechanical testing of the polyamides doped with 10 wt% DOPO-tethered salt against industrial PA66.

Table S1. Heat release rate (HRR) and other MCC data for polyamides.

	Char			HRR Max	Total
Samples	Yield	FGC	HRR Peak (s)	Temp	HR
-	(wt%)	(J/g-k)	(W/g)	(°C)	(kJ/g)

PA66	1.45	487	560	478	28.0
	1.40	485	560	482	28.2
	1.28	487	566	480	28.3
PA66	1.10	515			29.4
	1.19	521			29.2
	1.29	515			29.1
PA66-5B	1.74	333	374, 237	423, 487	28.0
	1.77	333	383, 243	422, 486	28.0
	1.67	326	388, 250	424, 490	27.8
PA66-5F	1.63	323	329, 228	430, 486	27.4
	1.70	329	338, 243	430, 488	28.0
	2.02	323	327, 230	427, 485	27.5
PA66-					
10B	1.55	335	315, 220	423, 487	27.7
	1.65	327	325, 217	424, 489	27.6
	1.55	324	384, 220	419, 490	27.6
	1.50	324	371, 223	421, 489	27.9
- 4 4 4 4 4 4 4 4 4 4 4 4 4 4 4 4 4 4 4					

^aAn additional replicate was run for PA66-10B sample due to the scatter in heat release data